ARL-TR-10369 ● JUNE 2026

Investigation of Laser Powder Bed Fusion of Magnesium Alloys

by Alexander Butler, Jian Yu, and Brandon McWilliams

NOTICES

Disclaimers

ARL-TR-10369 ● JUNE 2026

Investigation of Laser Powder Bed Fusion of Magnesium Alloys

Alexander Butler, Jian Yu, and Brandon McWilliams
DEVCOM Army Research Laboratory

REPORT DOCUMENTATION PAGE

1. REPORT DATE	2. REPORT TYPE	3. DATES COVERED START DATE	3. DATES COVERED END DATE
June 2026	Technical Report	14 November 2023	1 June 2026

4. TITLE AND SUBTITLE
Investigation of Laser Powder Bed Fusion of Magnesium Alloys

5a. CONTRACT NUMBER	5b. GRANT NUMBER	5c. PROGRAM ELEMENT NUMBER
5d. PROJECT NUMBER	**5e. TASK NUMBER**	**5f. WORK UNIT NUMBER**

6. AUTHOR(S)
Alexander Butler, Jian Yu, and Brandon McWilliams

7. PERFORMING ORGANIZATION NAME(S) AND ADDRESS(ES)	8. PERFORMING ORGANIZATION REPORT NUMBER
DEVCOM Army Research Laboratory ATTN: FCDD-RLA-MD Aberdeen Proving Ground, MD 21005	ARL-TR-10369

9. SPONSORING/MONITORING AGENCY NAME(S) AND ADDRESS(ES)	10. SPONSOR/MONITOR'S ACRONYM(S)	11. SPONSOR/MONITOR'S REPORT NUMBER(S)

12. DISTRIBUTION/AVAILABILITY STATEMENT
DISTRIBUTION STATEMENT A. Approved for public release: distribution unlimited.

13. SUPPLEMENTARY NOTES
ORCIDs: Alexander Butler, 0009-0002-3705-4961; Jian Yu, 0000-0002-1681-4602; Brandon McWilliams, 0000-0002-0494-3140

14. ABSTRACT
Laser powder bed fusion has the ability to create complex shapes that normally would not be possible with conventional manufacturing processes. Magnesium-based alloys are a structural material of interest due to their high strength-to-mass ratio. However, due to the reactive nature and density of magnesium powder, it can be difficult to manufacture with melting processes. This work describes the process optimization and characterization of three magnesium alloys (WE43, AZ91E, and EV31A), comparing their performance against material produce via conventional manufacturing techniques.

15. SUBJECT TERMS
laser powder bed fusion, LPBF, process optimization, magnesium alloys, lightweight alloys, mechanical testing, Sciences of Extreme Materials

16. SECURITY CLASSIFICATION OF: a. REPORT	b. ABSTRACT	C. THIS PAGE	17. LIMITATION OF ABSTRACT	18. NUMBER OF PAGES
UNCLASSIFIED	UNCLASSIFIED	UNCLASSIFIED	UU	23

19a. NAME OF RESPONSIBLE PERSON	19b. PHONE NUMBER *(Include area code)*
Alexander Butler	(520) 691-5564

STANDARD FORM 298 (REV. 5/2020)
Prescribed by ANSI Std. Z39.18

Contents

List of Figures

List of Tables

Acknowledgments

We thank Dr. Matthew Vaughn (Oak Ridge Associated Universities) for assistance in manufacturing and characterization of samples.

1. Introduction

Laser powder bed fusion (LPBF) is a common type of additive manufacturing (AM) in which a laser selectively melts layers of metal powder to yield nearly fully dense material. This process enables complex novel designs, especially those designed using topological optimization (TO). TO can yield a design, optimizing a given objective parameter; for example, maximizing stiffness or heat dissipation or minimizing vibration.[1–3] These designs are usually organic in nature, limiting the feasibility of using conventional manufacturing techniques.[4] AM has the agility to manufacture these complex designs without special tooling and limited postprocessing.

Frequently, one of the objectives of TO designs is to reduce volume and therefore weight of a given part. For these designs, it is natural to desire lightweight materials. Some TO designs utilize titanium alloys, frequently Ti-6Al-4V (Ti64) due to its high strength-to-weight ratio.[5,6] Other lightweight alloys, such as magnesium-based alloys, are also of interest but can be difficult to handle and manufacture.

Magnesium alloys' reactive nature requires extra precaution when handling and storing the powder. The powder is water-reactive and flammable, producing heat and hydrogen gas when exposed to water, causing numerous safety concerns. Additionally, the powder is hygroscopic, meaning moisture can be absorbed from the air and can cause powder clumping and flowability issues—both key characteristics for LPBF feedstock. Its microscopic size and light weight make them incredibly susceptible to air currents. LPBF systems use a constant gas flow across the powder bed to carry spatter particles away as they can land on solidified material and lead to defects.[7] The gas flow must be sufficient to carry spatter away from the powder bed and keep debris away from the laser window, which could obstruct exposure.[8] The gas flow near the flow outlet can carry powder away from the powder bed, causing short feeds and build failures and high material consumption. Lastly, magnesium has a low boiling point relative to its melting point.[9,10] As LPBF is a melting process, this yields a very tight processing window, where full melting and proper solidification can occur. Evaporation can lead to keyhole porosity and deviations in the chemical composition of the printed material compared with the feedstock. Proper process optimization is crucial for producing reliable, nearly fully dense material, to take advantage of novel lightweight designs.

2. Experimental

This work outlines the process optimization and characterization of three magnesium-based alloys produced via LPBF. The initial parameter sets investigated for the first alloy optimized (WE43), were selected after reviewing literature, as this alloy has shown promise for AM.[11,12] The optimization of the subsequent two alloys was informed by the results of the initial parameter search of WE43.

2.1 Feedstock

The alloys investigated were WE43, AZ91E, and EV31A. The powders were manufactured by Luxfer Inc. (United Kingdom), in a size range of 20–63 µm. Table 1 shows the typical compositions in weight percent for these alloys. Table 2 and Figure 1 show the size distribution measured via dynamic image analysis on the CAMSIZER X2. Before use, these powders sat in storage for between 1 to 5 years in a temperature-controlled conditioned environment with limited humidity and stored with desiccant. Nonetheless, there was some clumping of the powder and sieving the virgin powder through a 63-µm screen was done prior to first use as well as during reuse. Reused powder was blended with virgin powder during sieving to ensure even mixing.

Table 1. Compositions in weight percent of the alloys investigated (provided by Luxfer Inc.).

Alloy Powder name	WE43 MAP43	AZ91E MAP91	EV31A MAP21
Y	4%	. . .	. . .
Re	3%	. . .	. . .
Zr	0.5%	. . .	0.6%
Zn	. . .	0.5%	0.3%
Nd	. . .	. . .	2.7%
Gd	. . .	. . .	1.3%
Al	. . .	9.0%	. . .
Mn	. . .	0.2%	. . .
Mg	Balance	Balance	Balance

Table 2. Size distribution characteristics of powders.

Alloy Powder name	WE43 MAP43		AZ91E MAP91		EV31A MAP21	
	Reported	Measured	Reported	Measured	Reported	Measured
D_{10} (µm)	27	26.0	27	24.5	25	25.8
D_{50} (µm)	39	40.4	40	35.0	38	35.5
D_{90} (µm)	58	70.6	59	50.2	55	51.0

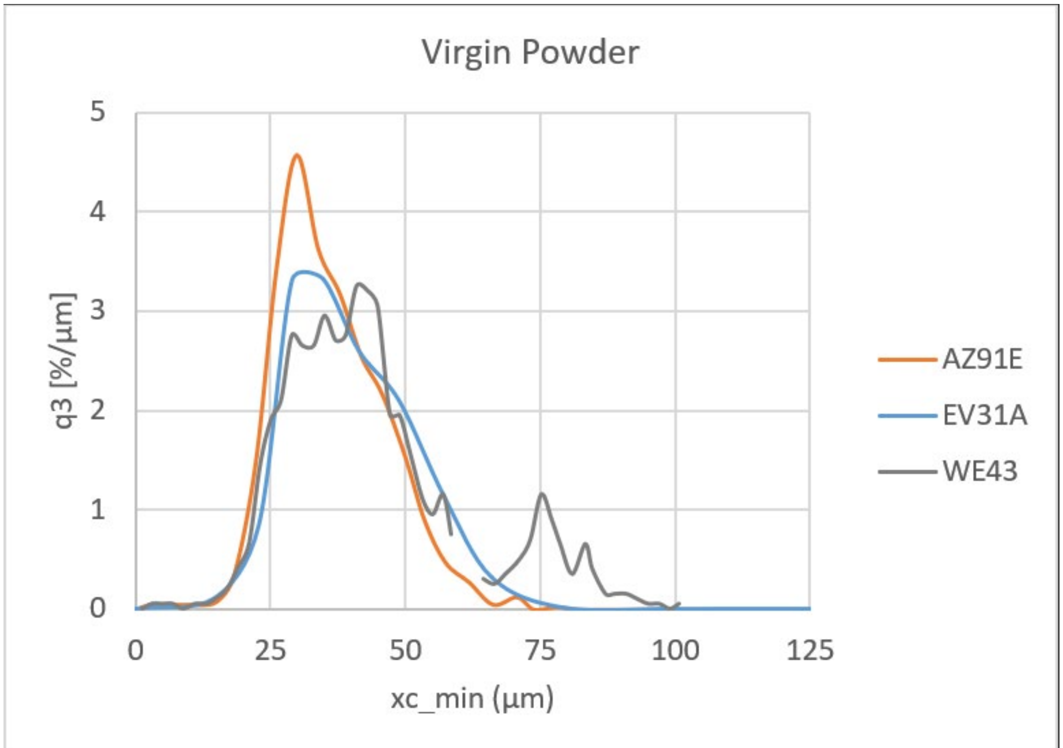

Figure 1. Particle size distribution of virgin magnesium alloy powder.

2.2 Manufacturing and Parameter Selection

The EOS M100 (Germany) LPBF system was used for this effort. The small build volume and ease of cleaning made it a good candidate for alloy development and process optimization. The system has a relatively low power laser, small spot size, and layer thickness, relative to those used in the literature referenced above. For these reasons, the process parameters in the literature could not be transferred one-to-one to this system. Volumetric energy density, E_v (J/mm^3) is used as a metric to compare processing parameters across parameter spaces and different LPBF systems.

$$E_v = \frac{P}{v*h*t} \quad (1)$$

where P is the laser power, v is the laser scan speed, h is the hatch spacing, and t is the layer thickness.[13] This calculated value is a more general term, quantifying the total energy input into the system, allowing an approximation of parameter sets. Based on the literature collected for WE43, a collection of 12 processing parameters was selected, with theoretical energy densities ranging from 28 to 42 J/mm^3 and averaging 35 J/mm^3. These 12 parameter sets will be referred to as the "initial parameter sets." During manufacture, the investigated parameter set was used for the infill, as well as the contour and upskin parameters.

2.3 Characterization

Cylinders (6-mm diameter and 10 mm tall) were printed for metallography and optical density measurements. After removal from the build plate via hand tools, these samples were sectioned, mounted, and polished to a 0.25-µm finish using an alcohol diamond suspension. All polishing lubricants and diamond suspensions used were alcohol-based, as water-based materials would react with the samples. These samples were imaged on a Keyence VHX7000 optical microscope. The micrographs were then converted to binary in ImageJ and a set of dilate and erosion sets were done to eliminate small polishing artifacts, like imbedded grit, from the pore analysis. For some WE43 samples, a Zeiss Xradia 5200, µCT was used to analyze the pore content of the material.

Once optimal processing parameters were identified based on optical density, 4-mm gauge subsize ASTM[14] E8 tensile bars were manufactured, in the horizontal orientation, perpendicular to the build direction. These samples were removed from the build plate via wire EDM and tested in the as-printed surface condition. The gauge sections were measured prior to testing on the Keyence VHX7000. These samples were tested on an Instron 5984 electromechanical load frame at a constant displacement rate of 1.0 mm/min with 3-D digital image correlation (DIC) to collect strain data.

3. Results

The optimized processing parameters along with their average density and mechanical properties are reported in Table 3. The complete datasets are included in the Appendix. In the case of WE43, no additional investigation was needed after the analysis of the initial parameter sets. For AZ91E, the initial parameter sets did not yield nearly fully dense material, and additional parameter sets were investigated. Lastly, for EV31A, the nine parameter sets, which yielded the best results for AZ91E were investigated.

Table 3. Optimized processing parameters with average density and mechanical performance.

Alloy	Powder name	Power (W)	Scan speed (mm/s)	Hatch spacing (µm)	Layer thickness (µm)	E_v (J/mm^3)	Average density (%)	Ultimate tensile strength (UTS) (MPa)	Yield strength (MPa)	Young's modulus (GPa)	Strain at failure
WE43	MAP43	100	1400	100	20	31	99.84	230	176	42	3.3
AZ91E	MAP91	40	600	40	20	83	99.81	243 ± 12	198 ± 0.5	40 ± 0.4	1.5 ± 0.4
EV31A	MAP21	40	200	40	20	280	99.80	156 ± 27	NA	39 ± 1	0.4 ± 0.1

3.1 Optical Density

An example metallography cylinders' build is shown in Figure 2. For each alloy, the optical density was measured in the XY plane. The density of the promising WE43 samples was further characterized via µCT. The optical porosity of the XY plane and the porosity calculated via µCT were averaged to yield the value reported in Table 3. The promising AZ91E and EV31A parameter sets were sectioned again and the XZ plane and optical density characterized. These XY plane and XZ plate densities were averaged to yield the values reported in Table 3. This difference in characterization was due to the limited availability of the µCT system. Micrographs of the polished XY plane of the three alloys with their optimized parameter sets are shown in Figure 3. Figure 4 shows micrographs of the XZ plane of AZ91E and EV31A, and Figure 5 shows some representative slices of the µCT scan of WE43. All three alloys achieved similar levels of porosity, and the micrographs show similar pore morphology and distribution.

Figure 2. Metallography cylinder build in AZ91E.

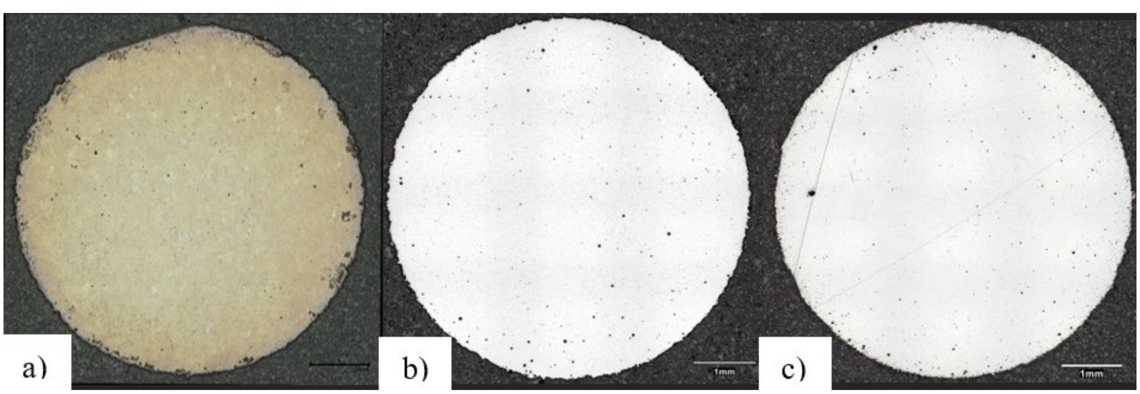

Figure 3. Micrographs of the XY planes for the densest samples of a) WE43, b) AZ91E, and c) EV31A.

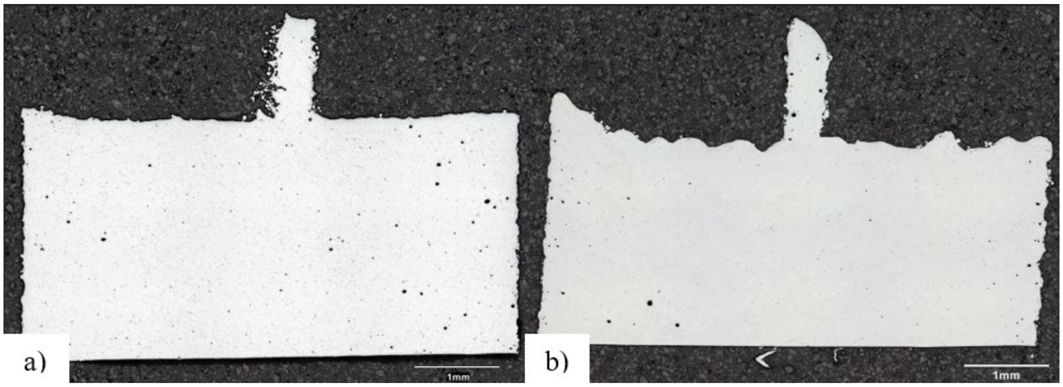

Figure 4. **Micrographs of XZ planes of a) AZ91E and b) EV31A.**

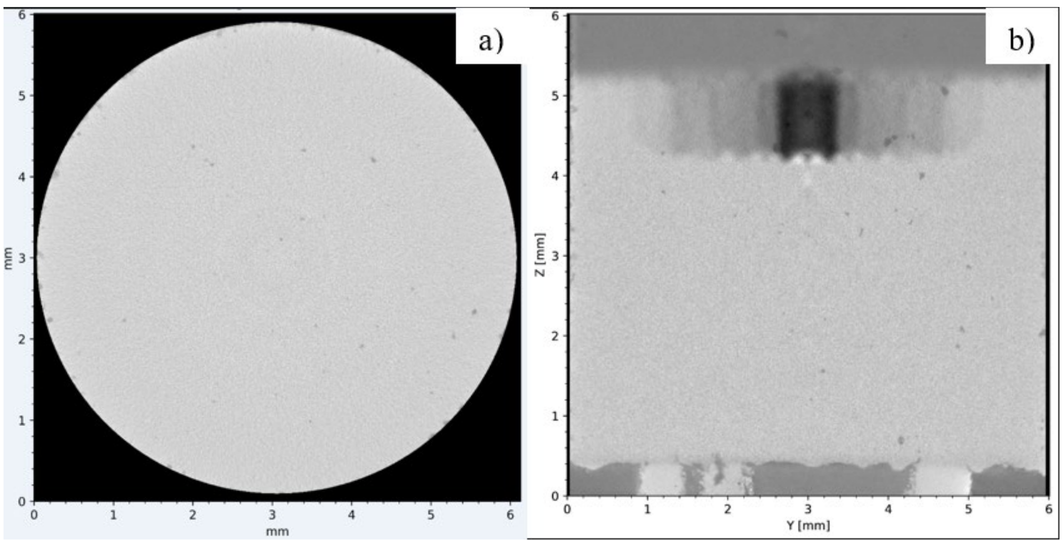

Figure 5. **µCT slices of WE43 in the a) XY and b) XZ planes.**

The XY plane density as a function of energy density is plotted in Figure 6. This shows significant differences in processing windows for these three alloys. WE43 achieves a high-density material in most parameter sets investigated; however, there is variation in density among parameter sets with similar energy densities.

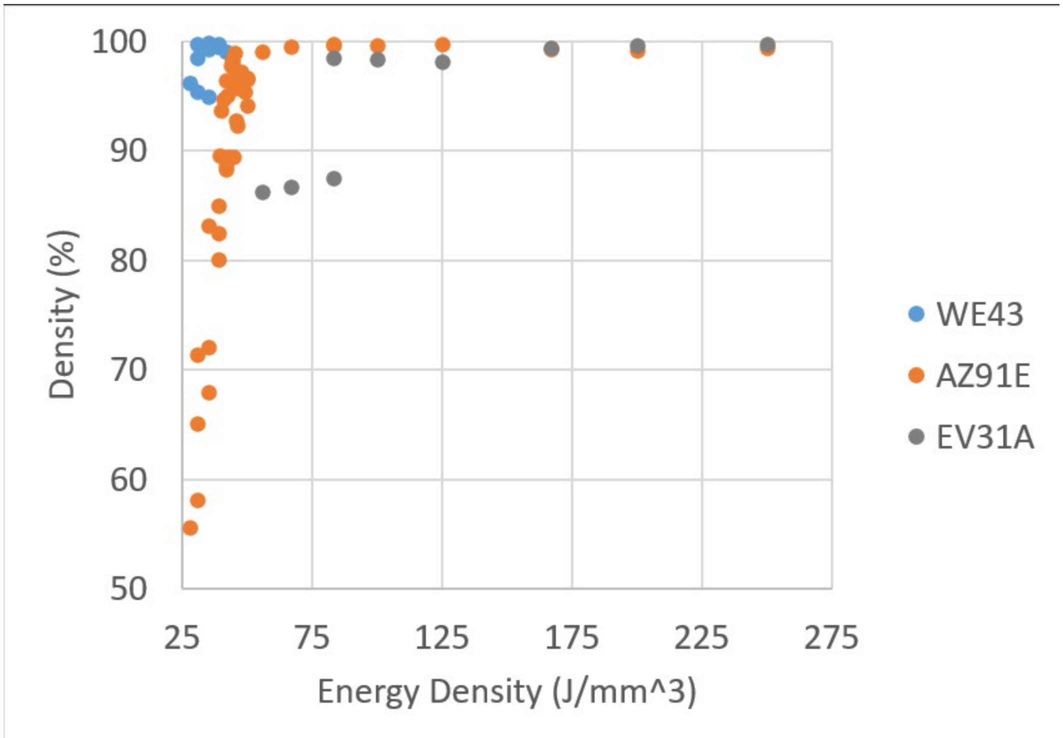

Figure 6. **Optical XY plane density as a function of energy density.**

During optimization of AZ91E, it was assumed the optimal energy density was near that of WE43, which is why the range of 25 to 42 J/mm^3 was so heavily investigated. After multiple iterations and only achieving <98% density, the energy density window to investigate was expanded. After which, it was seen that there appears to be a minimum energy density value of approximately 50 J/mm^3 that is required to produce >99% dense, after which there is a wide range of energy density values that produce nearly fully dense material.

EV31A appears to increase in density with increasing energy density, which is not observed in the other two alloys. It is assumed this relationship has an upper limit after which porosity due to keyholing will increase with increasing energy density.

3.2 Tensile Testing

Figure 7 shows an example build of the subsize tensile bars. Although little-to-no cracking was seen in the EV31A metallography cylinders, the tensile bars showed significant cracking along the loading direction of the tensile bar.

Figure 7. Subsize tensile bar build of EV31A.

Additionally, although the same processing parameters were used for all exposure regimes (infill, upskins, contours, etc.), significant geometric deviation was seen on the top of the samples—where the sides appear to be raised and the upskin seems to be rough. This phenomenon did not appear to have a correlation with positioning of the sample with regard to the gas flow or the recoater direction.

Figure 8 shows the tensile performance of the optimized parameter sets for each alloy. The measured mechanical properties are shown in Table 3 and are compared with material produced via conventional manufacturing methods in Table 4. For AZ91E and EV31A, the reported values are averaged from at least three tensile samples. As for WE43, the reported values are from a single sample. It is important to note that as the LPBF samples did not undergo any postbuild heat treatment, the “conventionally manufactured” material in Table 4 is also without any subsequent heat treatment or solution treatment. In almost all cases, these materials would undergo some aging or solution treatment. This was done to quantify the “virgin” material from the manufacturing methods, to make comparisons among the processes easier.

In the cases of WE43 and AZ91E, the LPBF samples achieved higher UTS, yield strength, and comparable or higher stain at failure. In the case of EV31A, the UTS and strain at failure are lower than the conventional counterparts.

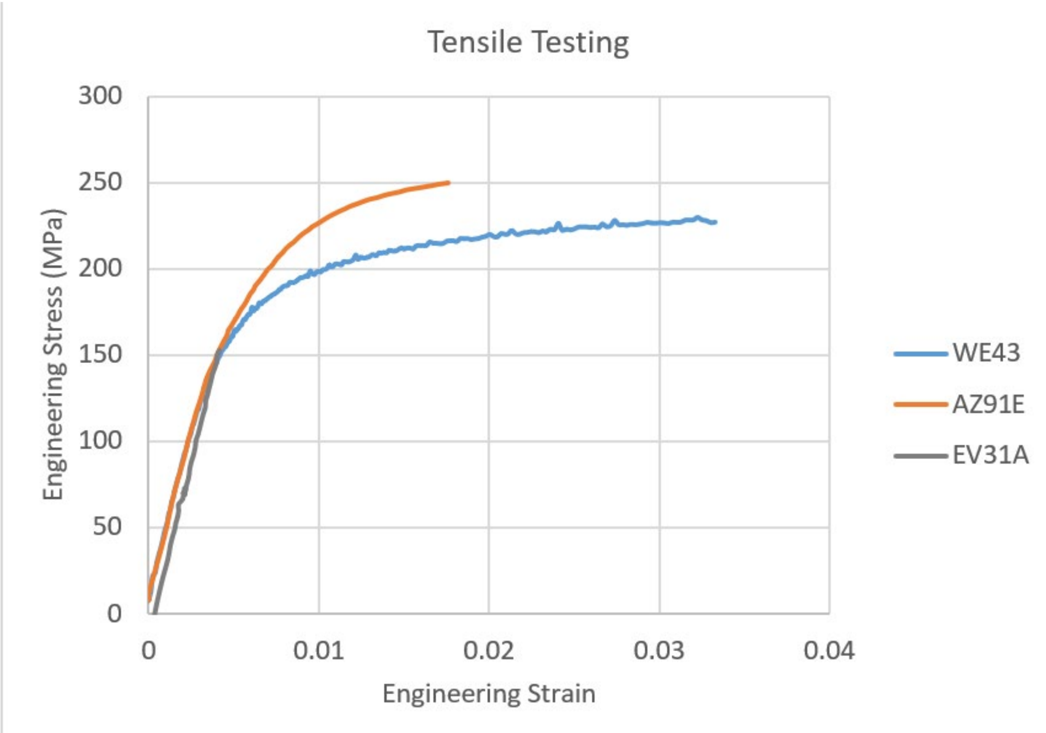

Figure 8. **Stress-strain curves of investigated magnesium (Mg) alloys.**

Table 4. **Comparison of LPBF samples with conventionally manufactured samples.**

Alloys	Manufacturing method	UTS (MPa)	Yield strength (MPa)	Strain at failure
WE43	As-cast[15]	171	126	1.5
	LPBF – this work	230	176	3.3
AZ91E	As-sand-cast[16]	128	102	1.1
	LPBF – this work	243 ± 12	198 ± 0.5	1.5 ± 0.4
EV31A	As-stir-cast[17]	192	130	7
	LPBF – this work	156 ± 27	NA	0.4 ± 0.1

4. Discussion

Near fully dense material was produced in metallography cylinders for all alloys. Tensile testing showed promising results for most of the alloys investigated. The UTS of WE43 and AZ91E saw increases of 34% and 90%, respectively, compared with the referenced material produced via conventional manufacturing methods. This, combined with the comparable or improved strain at failure and low porosity, indicates that the manufacturing of WE43 and AZ91E were both properly optimized and were manufactured with limited defects. The mechanical performance of LPBF WE43 and AZ91E differed slightly, with WE43 displaying over double the elongation than AZ91E while having slightly less strength. This demonstrates two possible performance and application spaces in which these alloys can be utilized.

As for EV31A, the cracks seen in the tensile coupons, the nonuniform upskins, and poor tensile performance indicate additional process optimization might have been necessary. It is important to note that the uneven surface of the EV31A tensile bars made it difficult to fixture in the grips of the load frame. It was necessary to lightly file the grip sections flat for better grip. Additionally, the higher surface roughness of the EV31A upskin compared with the other samples most likely introduced a significant amount of stress concentrations, leading to premature failure.

Due to the varying number of parameter sets investigated for each alloy, it is difficult to make fully informed comparisons of the processing windows for each alloy. AZ91E seemed to have a very broad processing window once the parameter sets yield energy densities above approximately 50 J/mm^3. However, density appears to decrease after approximately 84 J/mm^3. With EV31A, as mentioned previously, density increases with energy density. However, similar to AZ91E, there most likely exists an upper bound to this trend, where increasing energy density will yield to higher porosity.

Lastly, as mentioned, most magnesium alloys are used in their heat-treated state. This work is simply comparing the as-manufactured properties. As was shown, the mechanical performance of the LPBF WE43 and AZ91E was better than that of the referenced conventionally manufactured material and allows for the manufacture of parts that do not necessarily require subsequent heat treatment to achieve improved mechanical performance.

5. Conclusion

Magnesium alloys are intrinsically difficult to manufacture via melting processes. The density and reactivity of the powder create unique handling and processing concerns. This work highlights the successful optimization of the LPBF process for WE43 and AZ91E, which displayed improved tensile performance compared with some material manufactured via conventional processes. It is possible the poor performance of EV31A is due to the limited process optimization conducted here. Additional data points would need to be investigated to identify the effective processing window and ideal performance of this material.

6. References

1. Niu F, Xu S, Cheng G. A general formulation of structural topology optimization for maximizing structural stiffness. Struct Multidisc Optim. 2011;43:561–572. https://doi.org/10.1007/s00158-010-0585-8
2. Lohan DJ, Dede EM, Allison JT. A study on practical objectives and constraints for heat conduction topology optimization. Struct Multidisc Optim. 2020;61:475–489. https://doi.org/10.1007/s00158-019-02369-6
3. Zargham S et al. Topology optimization: a review for structural designs under vibration problems. Struct Multidisc Optim. 2016;53:1157–1177. https://doi.org/10.1007/s00158-015-1370-5
4. Ibhadode O et al. Topology optimization for metal additive manufacturing: current trends, challenges, and future outlook. Virtual Phys Prototyp. 2023;18.1:e2181192.
5. Yoder S et al. Characterization of topology optimized Ti-6Al-4V components using electron beam powder bed fusion. Addit Manuf. 2018;19:184–196. https://doi.org/10.1016/j.addma.2017.12.001
6. Vilardell AM et al. Topology optimization and characterization of Ti6Al4V ELI cellular lattice structures by laser powder bed fusion for biomedical applications. Mater Sci Eng A. 2019;766:138330. https://doi.org/10.1016/j.msea.2019.138330
7. Schwerz C et al. In-situ detection of redeposited spatter and its influence on the formation of internal flaws in laser powder bed fusion. Addit Manuf. 2021;47:102370. https://doi.org/10.1016/j.addma.2021.102370
8. Zhang X, Cheng B, Tuffile C. Simulation study of the spatter removal process and optimization design of gas flow system in laser powder bed fusion. Addit Manuf. 2020;32:101049. https://doi.org/10.1016/j.addma.2020.101049
9. Wan Harun W. A critical review of selective laser melting of magnesium and its alloys. Int J Adv Manuf Technol. 2025;140:4577–4623. https://doi.org/10.1007/s00170-025-16561-0
10. Hyer H et al. Additive manufacturing of dense WE43 Mg alloy by laser powder bed fusion. Addit Manuf. 2020;33:101123. https://doi.org/10.1016/j.addma.2020.101123

11. Zumdick NA et al. Additive manufactured WE43 magnesium: A comparative study of the microstructure and mechanical properties with those of powder extruded and as-cast WE43. Mater Charact. 2019;147:384–397. https://doi.org/10.1016/j.matchar.2018.11.011

12. Gangireddy S, Gwalani B, Liu K, Faierson EJ, Mishra RS. Microstructure and mechanical behavior of an additive manufactured (AM) WE43-Mg alloy. Addit Manuf. 2019;26:53–64. https://doi.org/10.1016/j.addma.2018.12.015

13. Zhao R et al. On the role of volumetric energy density in the microstructure and mechanical properties of laser powder bed fusion Ti-6Al-4V alloy. Addit Manuf. 2022;51:102605.

14. ASTM E8/E8M-22. Standard test methods for tension testing of metallic materials. ASTM International; 2024.

15. Jia G-L et al. Microstructure, mechanical properties and fracture behavior of a new WE43 alloy. Rare Metals. 2021;40:2197–2205. https://doi.org/10.1007/s12598-020-01423-3

16. Marodkar AS, Patil H, Chavhan J, Borkar H. Effect of gravity die casting, squeeze casting and extrusion on microstructure, mechanical properties and corrosion behaviour of AZ91 magnesium alloy. Mater Today Proc; 2023. https://doi.org/10.1016/j.matpr.2023.03.053

17. Somasundaram M, NarendraKumar U. Microstructural and mechanical properties of a heat-treated EV31A magnesium alloy fabricated using the stir-casting process. Crystals. 2022;12(8):1163. https://doi.org/10.3390/cryst12081163

Appendix. Complete Dataset

Table A-1. Full dataset of investigated parameter sets.

Sample ID	Alloy	Powder	Laser power (W)	Scan speed (mm/s)	Hatch spacing (um)	Spot size (um)	Layer thickness (um)	Energy density (J/mm^3)	Density (optical) XY plane (%)	Density (optical) XZ plane (%)	μCT density (%)	Young's modulus (GPa)	Ultimate tensile strength (MPa)	Yield strength (MPa)	Strain at failure (%)
1	WE43C	MAP43	100	1600	100	40	20	31	99.78	. . .	99.15	42	223	176	2.6
2	WE43C	MAP43	100	1400	100	40	20	35	99.91	. . .	99.84	42	230	176	3.3
3	WE43C	MAP43	100	1300	100	40	20	39	99.54	. . .	99.90	42	234	176	3.5
4	WE43C	MAP43	150	2700	100	40	20	28	96.27	. . .	97.24	38	182	147	1.8
5	WE43C	MAP43	150	2400	100	40	20	31	98.48	. . .	96.93	41	197	155	2.1
6	WE43C	MAP43	150	2100	100	40	20	35	99.32	. . .	97.56	40	215	169	3.0
7	WE43C	MAP43	150	1900	100	40	20	39	99.73	. . .	98.27	39	220	170	3.3
8	WE43C	MAP43	150	1800	100	40	20	42	99.11	. . .	98.75	42	223	168	3.3
9	WE43C	MAP43	170	2700	100	40	20	31	95.40	. . .	98.03	39	191	155	1.8
10	WE43C	MAP43	170	2400	100	40	20	35	94.99	. . .	97.96	39	201	164	2.4
11	WE43C	MAP43	170	2200	100	40	20	39	99.53	. . .	97.45	38	215	167	3.2
1_1	AZ91E	MAP91	100	1600	100	40	20	31	71.37	. . .	. . .	. . .	. . .	. . .	. . .
1_2	AZ91E	MAP91	100	1400	100	40	20	35	83.24	. . .	. . .	. . .	. . .	. . .	. . .
1_3	AZ91E	MAP91	100	1300	100	40	20	39	85.06	. . .	. . .	. . .	. . .	. . .	. . .
1_4	AZ91E	MAP91	150	2700	100	40	20	28	55.62	. . .	. . .	. . .	. . .	. . .	. . .
1_5	AZ91E	MAP91	150	2400	100	40	20	31	65.13	. . .	. . .	. . .	. . .	. . .	. . .
1_6	AZ91E	MAP91	150	2100	100	40	20	35	72.08	. . .	. . .	. . .	. . .	. . .	. . .
1_7	AZ91E	MAP91	150	1900	100	40	20	39	80.08	. . .	. . .	. . .	. . .	. . .	. . .
1_8	AZ91E	MAP91	150	1800	100	40	20	42	88.35	. . .	. . .	. . .	. . .	. . .	. . .
1_9	AZ91E	MAP91	170	2700	100	40	20	31	58.08	. . .	. . .	. . .	. . .	. . .	. . .
1_10	AZ91E	MAP91	170	2400	100	40	20	35	67.94	. . .	. . .	. . .	. . .	. . .	. . .
1_11	AZ91E	MAP91	170	2200	100	40	20	39	82.49	. . .	. . .	. . .	. . .	. . .	. . .
2_1	AZ91E	MAP91	80	800	100	40	20	50	96.53	. . .	. . .	. . .	. . .	. . .	. . .
2_2	AZ91E	MAP91	80	900	100	40	20	44	97.71	. . .	. . .	. . .	. . .	. . .	. . .
2_3	AZ91E	MAP91	80	1000	100	40	20	40	93.72	. . .	. . .	. . .	. . .	. . .	. . .
2_4	AZ91E	MAP91	100	1000	100	40	20	50	96.66	. . .	. . .	. . .	. . .	. . .	. . .
2_5	AZ91E	MAP91	100	1100	100	40	20	45	96.51	. . .	. . .	. . .	. . .	. . .	. . .
2_6	AZ91E	MAP91	100	1200	100	40	20	42	88.72	. . .	. . .	. . .	. . .	. . .	. . .
2_7	AZ91E	MAP91	120	1200	100	40	20	50	94.15	. . .	. . .	. . .	. . .	. . .	. . .
2_8	AZ91E	MAP91	120	1300	100	40	20	46	96.73	. . .	. . .	. . .	. . .	. . .	. . .
2_9	AZ91E	MAP91	120	1400	100	40	20	43	89.51	. . .	. . .	. . .	. . .	. . .	. . .
3_1	AZ91E	MAP91	60	850	80	40	20	44	98.18	. . .	. . .	. . .	. . .	. . .	. . .
3_2	AZ91E	MAP91	60	950	70	40	20	45	98.93	. . .	. . .	. . .	. . .	. . .	. . .
3_3	AZ91E	MAP91	60	1050	60	40	20	48	96.80	. . .	. . .	. . .	. . .	. . .	. . .
3_4	AZ91E	MAP91	80	800	110	40	20	45	96.13	. . .	. . .	. . .	. . .	. . .	. . .
3_5	AZ91E	MAP91	80	1000	90	40	20	44	98.31	. . .	. . .	. . .	. . .	. . .	. . .
3_6	AZ91E	MAP91	80	1100	80	40	20	45	95.80	. . .	. . .	. . .	. . .	. . .	. . .
3_7	AZ91E	MAP91	100	1000	110	40	20	45	92.76	. . .	. . .	. . .	. . .	. . .	. . .
3_8	AZ91E	MAP91	100	1400	80	40	20	45	89.50	. . .	. . .	. . .	. . .	. . .	. . .
3_9	AZ91E	MAP91	100	1200	90	40	20	46	92.29	. . .	. . .	. . .	. . .	. . .	. . .
4_1	AZ91E	MAP91	55	850	70	40	20	46	97.10	. . .	. . .	. . .	. . .	. . .	. . .
4_2	AZ91E	MAP91	55	925	70	40	20	42	95.09	. . .	. . .	. . .	. . .	. . .	. . .
4_3	AZ91E	MAP91	55	1000	70	40	20	39	89.63	. . .	. . .	. . .	. . .	. . .	. . .
4_4	AZ91E	MAP91	65	850	80	40	20	48	97.23	. . .	. . .	. . .	. . .	. . .	. . .
4_5	AZ91E	MAP91	65	925	80	40	20	44	97.87	. . .	. . .	. . .	. . .	. . .	. . .
4_6	AZ91E	MAP91	65	1000	80	40	20	41	94.77	. . .	. . .	. . .	. . .	. . .	. . .
4_7	AZ91E	MAP91	75	850	90	40	20	49	95.41	. . .	. . .	. . .	. . .	. . .	. . .
4_8	AZ91E	MAP91	75	925	90	40	20	45	96.07	. . .	. . .	. . .	. . .	. . .	. . .
4_9	AZ91E	MAP91	75	1000	90	40	20	42	96.45	. . .	. . .	. . .	. . .	. . .	. . .
5_1	AZ91E	MAP91	40	200	40	40	20	250	99.46	99.59	. . .	. . .	. . .	. . .	. . .
5_2	AZ91E	MAP91	40	400	40	40	20	125	99.74	99.70	. . .	. . .	. . .	. . .	. . .
5_3	AZ91E	MAP91	40	600	40	40	20	83	99.81	99.81	. . .	40	243	198	1.5
5_4	AZ91E	MAP91	40	200	50	40	20	200	99.23	. . .	. . .	. . .	. . .	. . .	. . .
5_5	AZ91E	MAP91	40	400	50	40	20	100	99.62	99.61	. . .	. . .	. . .	. . .	. . .
5_6	AZ91E	MAP91	40	600	50	40	20	667	99.56	99.76	. . .	. . .	. . .	. . .	. . .
5_7	AZ91E	MAP91	40	200	60	40	20	167	99.26	. . .	. . .	. . .	. . .	. . .	. . .
5_8	AZ91E	MAP91	40	400	60	40	20	83	99.60	99.71	. . .	. . .	. . .	. . .	. . .
5_9	AZ91E	MAP91	40	600	60	40	20	56	99.04	. . .	. . .	. . .	. . .	. . .	. . .
1_1	EV31A	MAP21	40	200	40	40	20	250	99.80	99.85	. . .	39	156	NA	0.4
1_2	EV31A	MAP21	40	400	40	40	20	125	98.16	. . .	. . .	. . .	. . .	. . .	. . .
1_3	EV31A	MAP21	40	600	40	40	20	83	87.54	. . .	. . .	. . .	. . .	. . .	. . .
1_4	EV31A	MAP21	40	200	50	40	20	200	99.69	99.75	. . .	. . .	. . .	. . .	. . .
1_5	EV31A	MAP21	40	400	50	40	20	100	98.38	. . .	. . .	. . .	. . .	. . .	. . .
1_6	EV31A	MAP21	40	600	50	40	20	67	86.71	. . .	. . .	. . .	. . .	. . .	. . .
1_7	EV31A	MAP21	40	200	60	40	20	167	99.47	99.73	. . .	. . .	. . .	. . .	. . .
1_8	EV31A	MAP21	40	400	60	40	20	83	98.54	. . .	. . .	. . .	. . .	. . .	. . .
1_9	EV31A	MAP21	40	600	60	40	20	56	86.30	. . .	. . .	. . .	. . .	. . .	. . .

List of Symbols, Abbreviations, and Acronyms

3-D	Three-Dimensional
AM	Additive Manufacturing
DIC	Digital Image Correlation
LPBF	Laser Powder Bed Fusion
Mg	Magnesium
NA	Not Applicable
Ti64	Ti-6Al-4V
TO	Topological Optimization
UTS	Ultimate Tensile Strength

1 (PDF)	DEFENSE TECHNICAL INFORMATION CTR DTIC OCA
1 (PDF)	DEVCOM ARL FCDD RLB CB TECH LIB